Biomaterials 163 (2018) 128–141

Contents lists available at ScienceDirect

Biomaterials

journal homepage: www.elsevier.com/locate/biomaterials

Biofunctionalized aligned microgels provide 3D cell guidance to mimic complex tissue matrices

Jonas C. Rose [1], David B. Gehlen [1], Tamás Haraszti, Jens Köhler, Christopher J. Licht, Laura De Laporte*

DWI – Leibniz-Institute for Interactive Materials, Aachen, Germany

ARTICLE INFO

Article history:
Received 19 August 2017
Received in revised form
1 February 2018
Accepted 2 February 2018
Available online 9 February 2018

Keywords:
Artificial extracellular matrix
Tissue regeneration
Injectable hydrogel
Anisotropy
Magnetic alignment
Microgels

ABSTRACT

Natural healing is based on highly orchestrated processes, in which the extracellular matrix plays a key role. To resemble the native cell environment, we introduce an artificial extracellular matrix (aECM) with the capability to template hierarchical and anisotropic structures *in situ*, allowing a minimally-invasive application via injection. Synthetic, magnetically responsive, rod-shaped microgels are locally aligned and fixed by a biocompatible surrounding hydrogel, creating a hybrid anisotropic hydrogel (Anisogel), of which the physical, mechanical, and chemical properties can be tailored. The microgels are rendered cell-adhesive with GRGDS and incorporated either inside a cell-adhesive fibrin or bioinert poly(ethylene glycol) hydrogel to strongly interact with fibroblasts. GRGDS-modified microgels inside a fibrin-based Anisogel enhance fibroblast alignment and lead to a reduction in fibronectin production, indicating successful replacement of structural proteins. In addition, YAP-translocation to the nucleus increases with the concentration of microgels, indicating cellular sensing of the overall anisotropic mechanical properties of the Anisogel. For bioinert surrounding PEG hydrogels, GRGDS-microgels are required to support cell proliferation and fibronectin production. In contrast to fibroblasts, primary nerve growth is not significantly affected by the biomodification of the microgels. In conclusion, this approach opens new opportunities towards advanced and complex aECMs for tissue regeneration.

1. Introduction

The extracellular matrix (ECM) of complex and aligned human tissues consists of highly ordered structural proteins. It provides both haptotactic guidance by biochemical gradients present in the ECM and durotaxic directionality via mechanical gradients or patterns [1–3]. To resemble endogenous microstructures of complex tissues, such as nerve, heart, or muscle, biomaterials have been spatially modified in their biochemical [4,5], physical [6], and mechanical [7] nature. However, many open questions remain to elucidate how much guiding cues are required in biomaterials to promote tissue formation. In one example, an artificial ECM (aECM) was engineered to mimic the fibrous native ECM through well-defined electrospun fibers [8]. Here, cell activity depended on the orientation, density, diameter, elasticity, and biochemical ligand density of the fibers, revealing the importance of cell mediated fiber recruitment. Yet, as in many other studies [9,10], cells were grown on top of the substrate, not fully mimicking the 3D native environment that a cell encounters in most tissues in the body.

To study cell behavior in a 3D aECM, hydrogels have been designed, in which cells can be mixed [11–19]. As this type of material can be injected as a liquid to sequentially crosslink into a 3D regenerative matrix, they provide great potential to be applied in a low invasive manner *in vivo*. Material injection eliminates the need for invasive surgical procedures, where tissue is removed to create space for an implant [20]. In sensitive tissues, such as the spinal cord, injectable hydrogels have been proposed to avoid further impairment after injury [20]. Due to their versatility, hydrogels can be modified with cell signaling and binding domains [22], as well as delivered with preloaded cells [23], growth factors [24], and vectors for genetic engineering [25–28]. While hydrogels made from natural proteins have an innate ability to degrade [29], hydrogels prepared from synthetic polymers can be rendered degradable via hydrolysis or enzymatic pathways to enable cell growth and migration. Synthetic advanced materials have been commonly modified with peptide sequences sensitive to matrix

* Corresponding author.
E-mail address: delaporte@dwi.rwth-aachen.de (L. De Laporte).
[1] Authors contributed equally.

https://doi.org/10.1016/j.biomaterials.2018.02.001

metalloproteinases (MMPs) to induce matrix degradation on cell demand [30]. The creation of these aECM hydrogels has provided injectable scaffolds, in which a 3D cell-induced remodeling process can take place towards native tissue [31].

Unfortunately, most injectable materials are still mainly isotropic, neglecting chemo-, mechano-, or haptotactic cell guidance, leaving a mismatch between endogenous anisotropic structural proteins and injectable biomaterials. In order to combine minimal invasiveness and oriented structures, only a few approaches have been investigated. In one example, patterns of biochemical signals were established inside a 3D hydrogel via light induced activation of an adhesive peptide, Arg-Gly-Asp (RGD), after implantation, demonstrating a regulatory effect on inflammation and vascularization *in vivo* [32]. In another approach, structural guidance has been achieved by self-assembling peptide amphiphiles forming oriented nanofibers *in situ*, inducing aligned cell and neurite growth [33]. Finally, external magnetic fields have been applied to obtain material anisotropy upon injection. Here, natural diamagnetic proteins or cellulose nanocrystals can be aligned in high magnetic fields (5–10 T) [34,35] or dispersed magnetic iron oxide nanoparticles can form polydisperse particle strings using low magnetic fields (<500 mT) to guide cells in a surrounding hydrogel [36–38]. However, in the latter, a large amount of iron oxide particles is required to form the strings and the dimensions of the strings are difficult to control.

In order to reduce the amount of iron oxide and control the properties of the guiding elements, we recently developed a hybrid material with the ability to fine-tune structural and mechanical anisotropy [39,40]. The resulting Anisogel triggered the cell's decision to grow in a unidirectional manner but the rod-shaped six-arm star-shaped poly(ethylene oxide-*stat*-propylene oxide)-acrylate (sPEG-A)-based microgels that were used as guiding elements were bioinert [39]. Surprisingly, the neurons grew in an aligned manner at very low concentrations of microgels (1 vol%) without being in direct physical contact with the microgels, indicating a strong impact of the anisotropic mechanical properties at a certain distance from the cells. In the case of aligned fibers, the effect of the interfiber distance above 2.5 μm inside a hydrogel matrix, has, to the best of our knowledge, not yet been studied systematically. In addition, it is unknown how much guidance cell and nerves really need to grow in an aligned manner, such as the effect of the presence of cell adhesive ligands on the fiber surface.

In this report, we developed an Anisogel, containing biomodified microgels to better template the cell niche of complex tissues and approximate the endogenous anisotropic proteins of a natural ECM (Fig. 1, left). This study enables us to investigate the importance of rendering the microgels cell adhesive by conjugating them with adhesive ligands. The Gly-Arg-Gly-Asp-Ser-Pro-Cys (**GRGDS**PC) peptide is coupled to the pre-polymer via Michael-type addition and superparamagnetic iron oxide nanoparticles (SPIONs) are mixed within the pre-polymer solution before in mold polymerization. The crosslinked microgels are magnetically aligned and embedded in two types of enzymatically crosslinking hydrogels: a natural fibrin gel and a synthetic bioinert PEG-based hydrogel (Fig. 1, middle/right). This comparison enables us to answer the question whether biofunctionalized microgels would provide sufficient support for aligned cell growth without a cell adhesive surrounding hydrogel. The extent to which the presence of adhesion moieties on the microgels influences their guiding effect and enhances their biocompatibility and remodeling capacity, is studied and compared.

2. Results and discussion

In order to fabricate a native-like aECM with a linear structure, bioactive, rod-shaped microgels are oriented inside a hybrid hydrogel. The microgels are fabricated by UV-crosslinking 20 wt/vol% sPEG-A using an in-mold polymerization technique, where the mold contains 5 by 5 by 50 μm^3 rectangular cavities. The sPEG-A is modified with the cell-adhesive peptide **GRGDS**PC via Michael-type addition to render the microgels bioactive (Fig. 2A). To analyze and optimize the conjugation of thiol-containing molecules, cysteine is initially coupled to sPEG-A. The decrease of thiols throughout the reaction, and thus the binding efficiency, is quantified by an Ellman's reagent, which forms a UV/VIS-active component in contact with thiols [41]. In accordance with literature [42], we observe a high pH dependency of the reaction with short reaction times of 2.5–3 min at pH 8.0, longer reaction times of 10 and 30 min for lower pH values of 7.4 and 7.0, respectively, and a very low reaction rate in the order of several hours for pH 6.0 (Fig. S1A). Based on the Ellman's assay, pH 7.4 and a reaction time of 10 min are chosen for further conjugations due to the short reaction time under physiological conditions. ^{1}H NMR analysis is applied in order to confirm the degree of cysteine functionalization (Fig. S2). For all cysteine concentrations, the experimental degree of functionalization corresponds to the amount of cysteine in the feed (Fig. S1B). As a sufficient number of free acrylate groups has to remain available for crosslinking, not all sPEG-A arms are biofunctionalized to produce the microgels. To vary the GRGDS concentration, while ensuring a homogeneous ligand distribution, sPEG-A with approximately 1

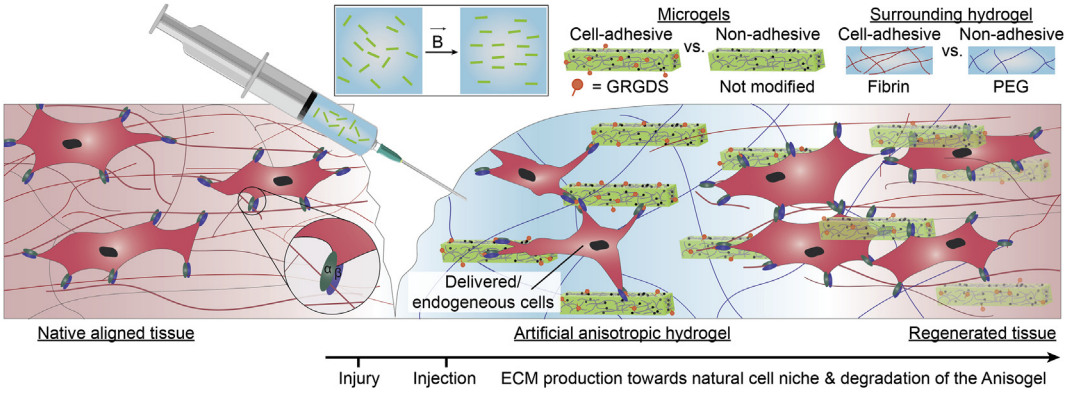

Fig. 1. (left) Schematic of the native complex structure of an ECM, which strongly interacts with the cells via the formation of focal adhesions (highlighted). In case of an injury, the liquid Anisogel precursor is injected (middle) and the cell-adhesive microgels are aligned in a magnetic field, followed by fixation via *in situ* crosslinking of the surrounding hydrogel. This hydrogel can be cell-adhesive (fibrin) or non-adhesive/bioinert (PEG). Remodeling of the synthetic aECM towards a native ECM (right), induced by the growing cells, while the microgels and hydrogel degrade over time.

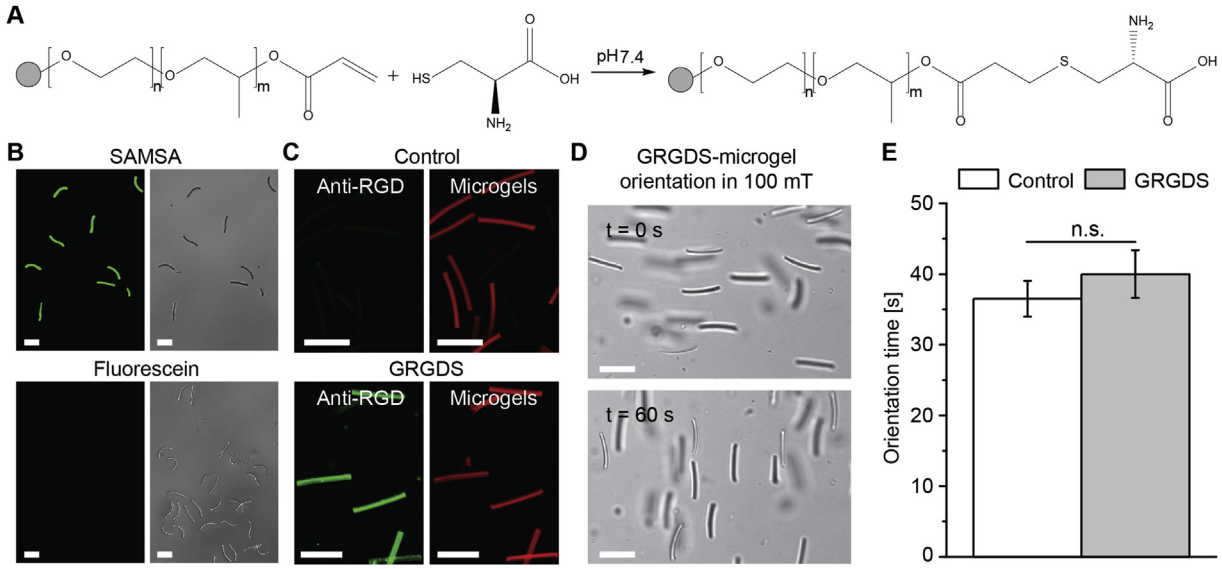

Fig. 2. A) Thiol-Michael addition of cysteine to the acrylate group of sPEG-A (displayed for one arm of the star polymer as an example). B) Microgels with SAMSA-fluorescein functionalized sPEG-A (top) show a strong fluorescence signal (green), whereas PEG-A, mixed with fluorescein without a thiol moiety (bottom), results in non-fluorescent microgels, demonstrating that all fluorescein is washed out. C) Non-modified (top) control microgels and GRGDS-coupled (bottom) microgels are immunohistochemically stained with an anti-RGD antibody, showing homogeneous GRGDS incorporation throughout the microgels (green: Alexa Fluor 488). The microgels are fluorescently labeled with rhodamine B (red). The exposure time (B) and laser intensity/detector sensitivity (C) are kept constant to ensure comparability. D) Rotation of GRGDS-coupled microgels of 90° within 60 s in 100 mT. E) The orientation time of GRGDS-microgels does not significantly differ from control microgels ($p > 0.05$), allowing orientation in 100 mT within less than 1 min ($n = 4$). Scale bars are 50 μm. (For interpretation of the references to color in this figure legend, the reader is referred to the Web version of this article.)

GRGDS-labeled arm (sPEG-GRGDS; 17.8% of the available acrylate groups are statistically functionalized with the biomolecule) is mixed at different weight ratios with unlabeled sPEG-A. For example, a 1:50 ratio results in 5 μmol GRGDS/g sPEG, which is diluted to a 20 w/vol% polymer solution before crosslinking, resulting in a final GRGDS concentration of 1 mM.

The incorporation of thiol-containing biomolecules into the microgel network is visualized by mixing fluorescein with and without a thiol with sPEG-A at a molar ratio of 1:4.7 before dilution and crosslinking. After microgel molding and purification, fluorescent microgels are acquired in the case of thiol-containing fluorescein (5-((2-(and-3)-S-(acetylmercapto) succinoyl) amino) fluorescein, SAMSA), while standard fluorescein is not coupled to the network and washed out, leaving non-fluorescent microgels behind (Fig. 2B). In addition, microgels prepared with 1 mM GRGDS demonstrate a homogeneous modification of the polymer network with GRGDS (Fig. 2C). Besides the incorporation of GRGDS, we confirm that SPIONs (400 μg/mL) are successfully embedded into the biofunctionalized microgels, rendering them responsive to an external magnetic field of 100 mT. The microgels orient within one minute, which is comparable to the response time of bioinert magneto-responsive microgels (Fig. 2D, E, Fig. S3) [39]. Finally, we demonstrate that the biofunctionalization does not significantly affect the microporous structure of the microgels using cryo-field emission scanning electron microscopy (FE-SEM imaging) (Fig. S4). These results show that biomolecules can successfully be tethered to microgels with a controlled functionalization degree by conjugating them to the pre-polymer before gelation.

As GRGDS has no complex tertiary structure, we do not observe effects of deactivation or denaturation by washing with acetone or ethanol during the purification of the microgels (data not shown). Since the microgels are prepared by curing sPEG-A using UV irradiation, we also tested the UV stability of GRGDS by coupling it to a sPEG-isocyanate hydrogel film as previously described [43]. We thereby prove that 1 h of UV exposure does not affect the activity of the peptide, resulting in unchanged growth of fibroblasts (Fig. S5). Moreover, we confirm that sPEG-A hydrogels do not release any cytotoxic compounds into the media via an indirect MTS assay ((3-(4,5-dimethylthiazol-2-yl)-5-(3-carboxymethoxyphenyl)-2-(4-sulfophenyl)-2H-tetrazolium). Media is incubated with (conditioned media) or without (incubated media) a hydrogel at 37 °C for 3 days and sequentially applied to culture cells. No differences in the MTS signal or morphology/spreading are observed, in comparison to fresh media (Fig. 3A and B).

To optimize the cell-adhesive peptide content in the sPEG network, the metabolic activity (MTS assay) and attachment (Live/Dead analysis) is measured for different GRGDS concentrations ranging from 0.25 to 4 mM. Fibroblasts are cultivated for 3 days on top of the sPEG-hydrogels, fabricated with the same composition as the microgels (Fig. S6). The metabolic activity increases with higher GRGDS concentrations from $24.7 \pm 8.4\%$ without GRGDS to $83.6 \pm 4.4\%$ at 1 mM GRGDS, compared to standard tissue culture polystyrene as a positive control (Fig. 3C). Higher concentrations do not further improve the metabolic activity. Furthermore, we observe that cells tend to form clusters without GRGDS, whereas they spread on the hydrogel surface at GRGDS concentrations at and above 1 mM GRGDS. A Live/Dead assay after 3 days reveals viable adhered cells in the case of GRGDS modification, whereas only very few cells survive on the control surfaces without GRGDS (Fig. 3D). As the fibroblasts do not infiltrate the microgels of the Anisogel but rather interact with them in a 2D manner, we continue with a peptide concentration of 1 mM GRGDS for the biofunctionalization of the microgels.

Rod-shaped soft microgels, supplemented with a low amount of SPIONs, allow magnetic ordering within ~40 s, with or without modification with cell adhesive moieties (Fig. 2D and E). After alignment, a surrounding soft hydrogel retains the microgel orientation and position 2 min post-injection to induce directed cell growth in a minimally invasive manner (supporting video 1). Using sPEG-A molecules offers the advantage to slowly hydrolyze the hydrogels via ester bonds, while their degradation products have a suffciently small hydrodynamic radius to allow elimination

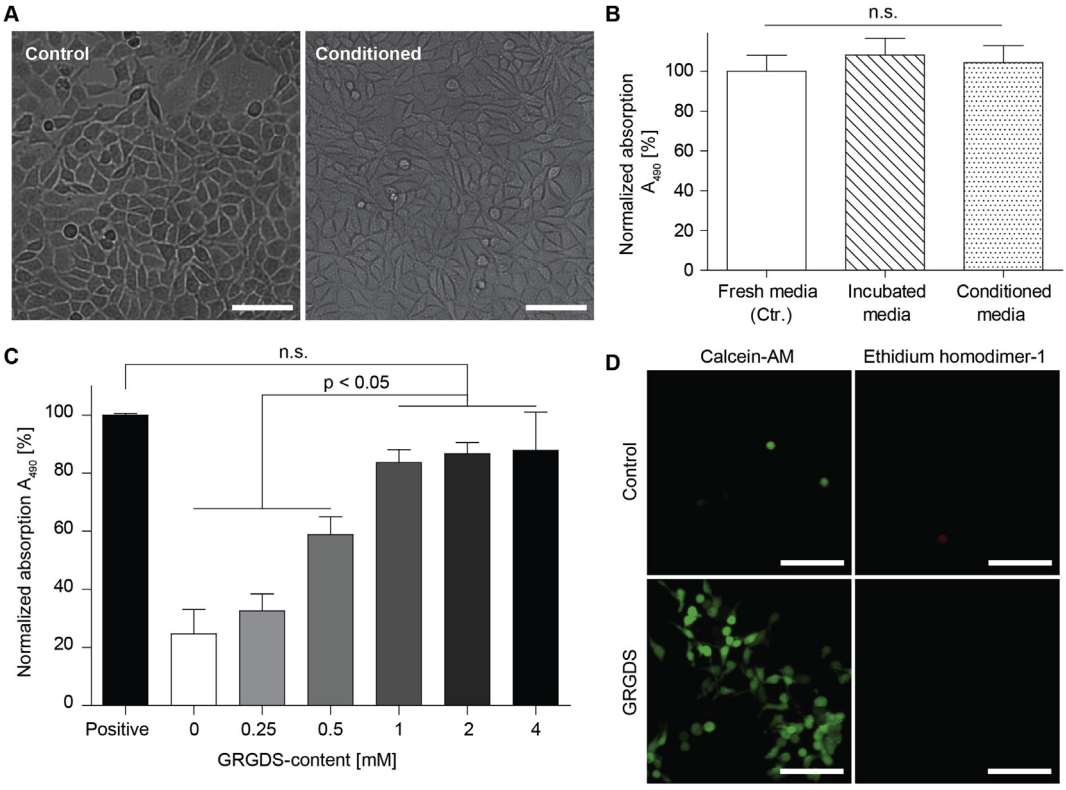

Fig. 3. A) Fibroblasts cultivated with fresh media and conditioned media, which is pre-incubated with an sPEG gel, showing no difference in cell morphology and spreading. B) Normalized absorption at 490 nm of fibroblasts based on a MTS assay, cultivated with fresh, incubated, and conditioned media show no significant differences, indicating that sPEG gels do not release any cytotoxic compounds (initial seeding: ~5000 cells, n = 3). C) Normalized absorption at 490 nm of fibroblasts (based on an MTS assay), cultivated on sPEG gels with different amounts of GRGDS, demonstrating a positive effect by incorporation of the peptide, but no further improvement for concentrations above 1 mM GRGDS (initial seeding: ~25,000 cells; n = 3). D) Live/Dead images of fibroblasts on sPEG gels without (top) and with 1 mM GRGDS (bottom). Green color: calcein-AM (Live), red color: ethidium homodimer-1 (Dead); Data presented as average ± s.d. and statistical significance performed using one-way ANOVA with Bonferroni comparison (n.s. = $p > 0.05$). Scale bars are 100 μm. (For interpretation of the references to color in this figure legend, the reader is referred to the Web version of this article.)

of the molecules through the kidney. During microgel degradation, very small amounts of SPIONs will be released over time, which can be processed by the native clearance and immune system. In order to study the effect of biofunctionalization of the microgels on cell growth, we first incorporate 0.5–2.0 vol% GRGDS-coupled or bioinert microgels within a fibrin precursor solution. Gelation of the fibrin takes place within a low external magnetic field (150 mT), creating a universal directionality of the magneto-responsive, rod-shaped microgels. Fibroblasts, mixed with cell-adhesive microgels strongly interact with the microgels, emulating the interaction of cells with the structural proteins of the native ECM. Thereby, an anisotropic aECM is produced, which mimics the cellular micro-environment of complex aligned tissues. In the case of GRGDS-microgels, the cells have a significantly larger contact area with the microgels compared to the bioinert microgels (Fig. 4A and Fig. S7, supporting video 2 and 3). Quantification of the 2D contact area between the cells and microgels elucidates that 28.9 ± 14.7% of the fibroblast area is in contact with the GRGDS coupled microgels, in comparison to 18.4 ± 9.8% for bioinert microgels (Fig. 4B). This substantiates the aspired strong interaction between cells and the created aECM. Furthermore, we observe strong stress fiber (F-actin) signals (Fig. 4A) and significantly more stretched cell nuclei in the case of biofunctionalized microgels compared to the bioinert ones, which is quantified by image-based analysis (Fig. 4C). This indicates that the cytoskeleton exerts a higher force on the nuclei [44]. We hypothesize that this phenomenon may be induced by the higher local stiffness of the microgels (E = 7.3 ± 1.6 kPa) compared to the surrounding hydrogel (E = 1.6 ± 0.4 kPa) (Fig. S8). The fibroblasts interact more strongly with the stiff microgels when these are cell-adhesive, while in the case of bioinert microgels, the cells interact more with the soft fibrin matrix. This is in agreement with previous reports where fibroblasts, cultured on stiffer surfaces (E ≥ 5 kPa), exhibit a more spread morphology with pronounced cytoskeletal stress fibers, which exert a force on both the nucleus and integrin clusters [45–47]. Strikingly, the fibroblasts mostly prefer to interact with GRGDS-microgels over the surrounding fibrin matrix, which itself has two cell adhesive RGD-sequences in the Aα-chain (at Aα572–575 (RGDS) and Aα95–98 (RGDF)) [48]. This may be explained by the higher stiffness of the microgels or the larger ligand density of GRGDS on the microgels (1 mM RGD), compared to the fibrin hydrogel (~50 μM RGD), enabling a strong integrin-mediated interaction [49]. Nevertheless, it is still interesting that cells rather adhere to the bioactive microgels than to the fibrin matrix, as fibrin contains many other cell binding sites besides RGD [50] and additional binding sites for other ECM proteins, such as fibronectin [51] or growth factors [52], inducing synergistic effects [53].

Supplementary video related to this article can be found at https://doi.org/10.1016/j.biomaterials.2018.02.001.

Next, the effect of the anisotropic aECM on the cells' cytoskeleton and its capability to induce unidirectional cell growth are analyzed. The presence and orientation of both bioinert and biofunctionalized microgels creates a material anisotropy, which triggers the fibroblasts' decision to grow in a unidirectional manner. In fibrin hydrogels without incorporated microgels, fibroblasts only grow randomly (Fig. S9). Initially, an F-actin image-

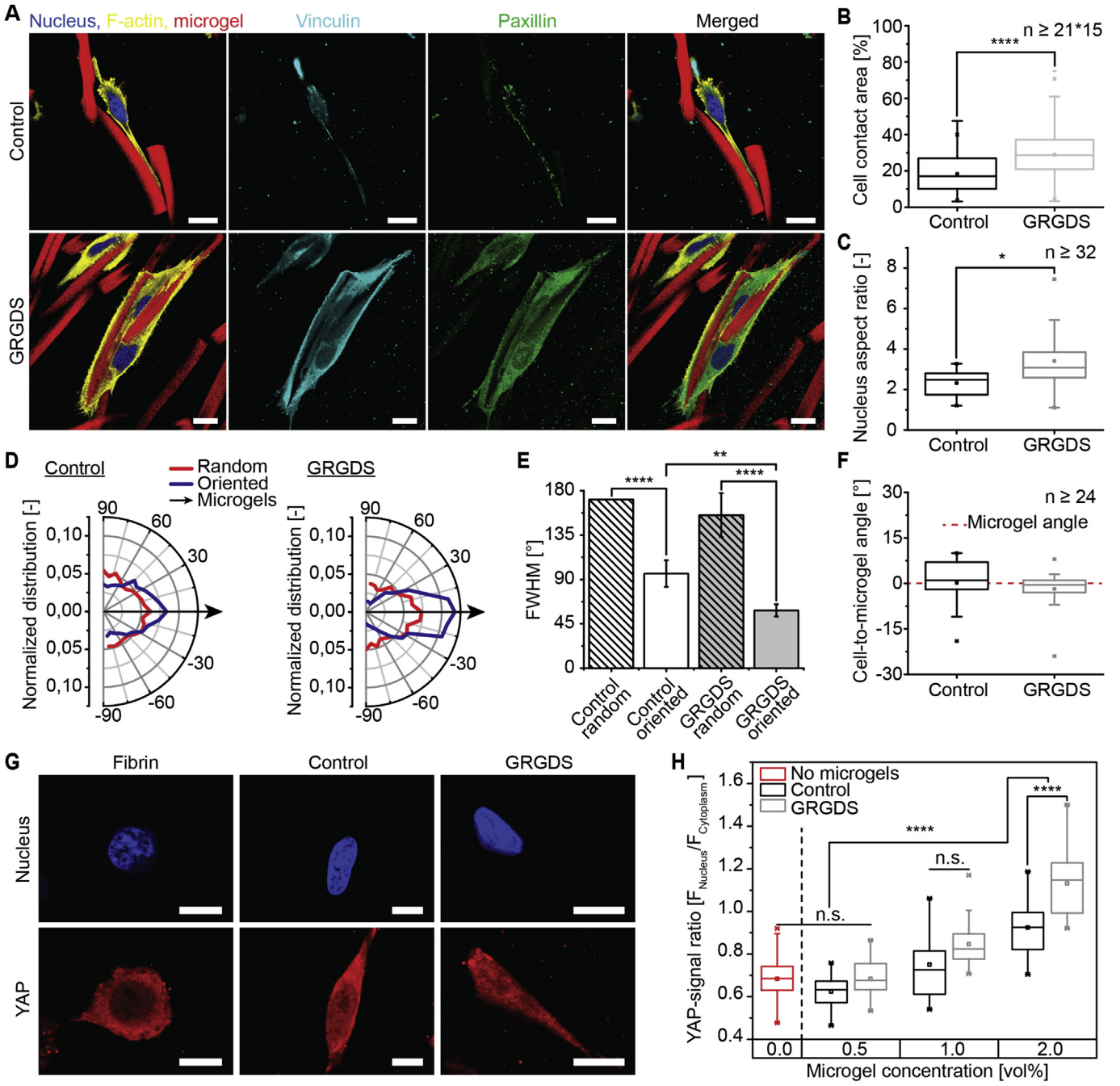

Fig. 4. A) Aligned and elongated cells interact less with bioinert microgels compared to biofunctionalized microgels. Blue: nucleus, yellow: F-actin, red: microgels, turquoise: vinculin, green: paxillin. B) Quantification of the cell contact area with the microgels. C) Aspect ratio (elongation) of the nucleus (DAPI) for cells in contact with bioinert (control) or biofunctionalized microgels inside the Anisogel. D) Normalized distribution of the overall cell orientation (F-actin) by image based analysis. Microgel orientation is indicated by the black arrow. E) Full width at half maximum (FWHM) of F-actin signal distributions, as represented in D, of three confocal stacks. F) Box plot diagram of the angle difference between the longest cell axis and the closest microgel long axis. G) YAP (red) is primarily located in the cytoplasm in fibrin hydrogels, while the addition of 2 vol% microgels induces shuttling towards the nucleus. H) Quantification of the YAP-signal ratio of the nucleus-to-cytoplasm, depending on the GRGDS modification of the microgels and the concentration of the microgels inside the Anisogel (n ≥ 20 cells). Scale bars are 10 μm. Data presented as average ± s.d. and statistical significance performed using a one-way or two-way ANOVA with Bonferroni comparison (*p < 0.05; **p < 0.01; ****p < 0.0001; n.s. = p > 0.05). (For interpretation of the references to color in this figure legend, the reader is referred to the Web version of this article.)

analysis is performed to quantify the aspect ratio of the cells (Fig. S10A). Here, we find a slight increase in aspect ratio in the case of GRGDS-modified microgels but cannot resolve significant differences between the microgel types. In order to increase the analysis sensitivity, the distribution of overall cell orientation is investigated, demonstrating cell alignment for both unmodified and biofunctionalized microgels (Fig. 4D). Yet, GRGDS-coupled microgels result into a narrower distribution (full width at half maximum (FWHM)) of cell alignment, indicating better cell orientation (Fig. 4E and Fig. S11). We hypothesize that the strong interaction of the cells with the microgels enhances the sensing of the material anisotropy. In comparison, cells in Anisogels with bioinert microgels interact more with their surrounding hydrogel, slightly reducing their unidirectional orientation. In order to

substantiate this hypothesis, cell alignment is analyzed relative to the direction of the neighboring microgel by determining the angle difference of the longest cell axis with the closest microgel long axis (Fig. 4F and Fig. S10B). Here, too, we observe a narrower angle distribution for GRGDS-coupled microgels in comparison to bioinert microgels.

In order to gain insight into the guidance and mechanobiological effect of the Anisogel on the cells, we stained for the intracellular Yes-associated protein (YAP). Shuttling of YAP/TAZ (transcriptional co-activator with PDZ-binding motif) between the nucleus on stiff substrates and the cytoplasm on soft substrates influences the cellular mechanical response by the level of expression of actin and related proteins, which form stress fibers [54]. Thus, the YAP signal is an important sensor of mechanotransduction, which we compared for fibroblasts inside the Anisogels versus a standard fibrin gel (Fig. 4G). Interestingly, the presence of aligned microgels (2 vol%) inside the Anisogel induces shuttling of YAP into the nucleus, in contrast to a clear YAP localization in the cytoplasm when cells are grown inside the soft fibrin gel. Furthermore, in case of GRGDS-coupled microgels, a significantly increased YAP signal is observed in the nucleus in comparison to bioinert microgels (Fig. 4H), which supports the observation of enhanced cellular guidance of fibroblasts for GRGDS-modified microgels. Supplying lower concentrations of microgels at 0.5 and 1 vol% decreases the YAP nucleus signal, even in direct contact with the stiff microgels (Fig. S12). This suggests that YAP translocation from the cytoplasm to the nucleus is strengthened by a strong interaction of the cells with RGD-modified microgels but also by the overall mechanical anisotropy of the Anisogel, which is sensed by the cells at a longer distance.

As cells are able to produce their own natural ECM over time to replace the artificial microenvironment, the amount and orientation of fibronectin, produced by the fibroblasts, is quantified after 48 h of cultivation inside the anisotropic hydrogels. Immunohistochemical staining and image-based analysis reveal that this fibronectin is aligned along the microgel orientation (Fig. 5A,B, Fig. S13, other microgel concentrations Fig. S14). In the case of 3D fibrin-based Anisogels, the fibronectin signal per cell with different microgel concentrations of 0.5, 1.0, and 2.0 vol% demonstrate that the amount of produced fibronectin is increased for bioinert

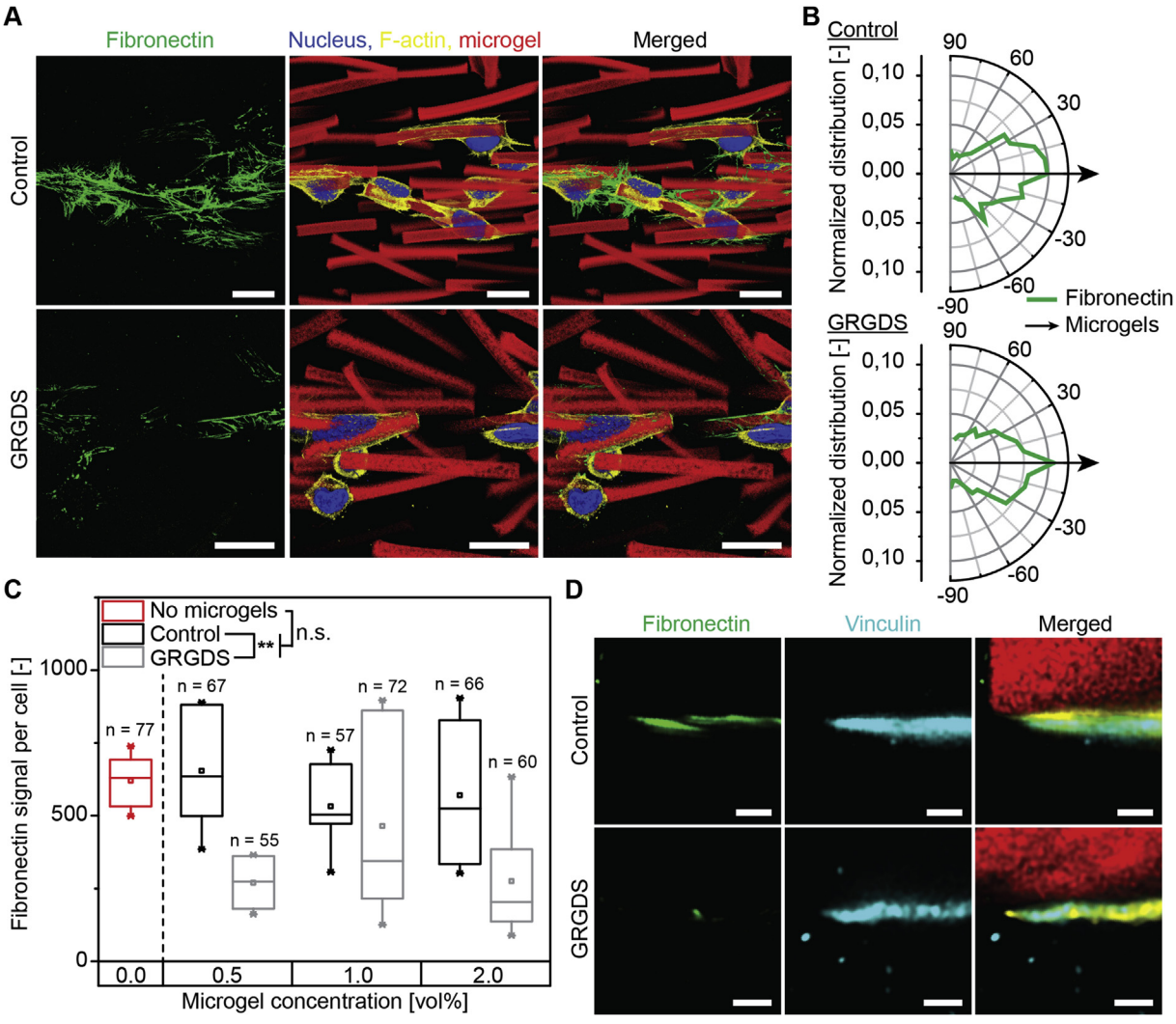

Fig. 5. A) Inside a fibrin-based Anisogel, fibronectin synthesis depends on the biofunctionality of the microgels. B) Distribution of orientation of the produced fibronectin (green), depending on the biofunctionality of the microgels (orientation indicated by black arrow). C) Box plot of the produced fibronectin per cell in 3D (n = number of analyzed cells) shows a higher value in the case of bioinert microgels, compared to bioactive microgels. D) Staining against vinculin reveals that the produced fibronectin overlaps with the signal for focal adhesion (control), whereas the bioactive microgels show focal adhesions of the cell in contact with the microgels without produced fibronectin. Data presented as average ± s.d. and statistical significance performed using a two-way ANOVA with Bonferroni comparison. Blue: nucleus, yellow: F-actin, red: microgels, turquoise: vinculin, green: fibronectin. Scale bars are 20 μm in A and 2 μm in D. (For interpretation of the references to color in this figure legend, the reader is referred to the Web version of this article.)

microgels, compared to fibrin only and GRDGDS-modified microgels (Fig. 5C). These results are confirmed by UV/VIS fluorescence measurements of five central areas of the overall Anisogel (Fig. S15). The stronger cell adhesion of fibroblasts to the GRGDS-coupled microgels seems to normalize the synthesis of fibronectin, similar to fibrin only, while cells are prompted to produce more fibronectin in the case of bioinert microgels to sufficiently adhere to the 3D anisotropic surrounding. These results support that the GRGDS-microgels contribute to the replacement of guiding adhesive structural proteins. Staining against the focal adhesion protein vinculin reveals that the focal adhesions are in direct contact with the biofunctionalized microgel surface with little fibronectin being produced (Fig. 5D). On the other hand, cells grown inside an Anisogel with bioinert microgels show an overlap of vinculin with the produced fibronectin. These results validate the strong adhesion of cells to the biofunctionalized microgels, whereas cells close to bioinert microgels have to produce their own ECM/fibronectin in order to attach to the microenvironment. These observations are in agreement with previous reports, where a decrease in collagen production by chondrocytes was observed when the amount of RGD inside a hydrogel was increased [55]. However, little has been reported about the influence of the type of hydrogel, cells, culture conditions, and the bio-modification of the aECM on the level of native ECM production and its distribution inside 3D scaffolds, which is a crucial aspect for tissue maturation in regenerative constructs.

As fibrin hydrogels are known to be cell-adhesive, we decoupled the matrix-cell and microgel-cell interactions by applying an inert but biocompatible PEG-based hydrogel to embed the microgels. The application of PEG as a surrounding matrix excludes any kind of biochemical interaction with the cells, revealing the pure effects of GRGDS microgel modification on the cell-microgel interactions and consequent cellular behavior. In addition, this enables us to study whether biofunctionalized microgels could provide sufficient support for aligned cell growth when surrounded by a bioinert hydrogel. The synthetic PEG-based hydrogel is crosslinked via the same enzymatic mechanism as fibrin [56]. It contains an MMP cleavable peptide sequence (GPQG↓IWGQ) in the backbone, allowing on cell-demand degradation. Yet, we did not add any bioadhesive molecules in order to suppress cell-matrix interactions. For this reason, only a few spherical cells are observed when bioinert microgels are incorporated, whereas more cells can attach and spread in hydrogels containing biofunctional microgels, which support cell adhesion to their surface (Fig. 6A). As PEG does not contain any growth factor binding sites in comparison to fibrin [52] and is protein repelling, serum-containing signaling molecules are not likely to locally promote cell proliferation. Cells spread parallel to the long axis of the biofunctional microgels with high densities of the focal adhesion proteins vinculin and paxillin in contact to the microgels. In these synthetic Anisogels, cell proliferation is reduced and almost no fibronectin is produced when bioinert microgels are applied. In the case of biofunctional microgels, adhesion sides are locally provided to enhance the proliferation of cells, which produce fibronectin and support each other forming multi-cellular structures (Fig. 6B). These results are in agreement with a previous report that demonstrated an increase in fibronectin production by valve interstitial cells grown in a PEG hydrogel at higher RGDS concentrations [57]. It emphasizes that the ECM production is highly dependent on the biochemical surrounding matrix and indicates a high complexity of the restoration process and the role of native ECM production in an artificial scaffold. However, the inertness of the PEG hydrogel does not support the formation of focal adhesions with the surrounding matrix, resulting in an incapability of the cells to sense the material's mechanical anisotropy and induce aligned cell growth. Only in direct contact with the bioactive microgels, cells can extent and align along the unidirectional microgels. In contrast to the fibrin-based Anisogels, a surrounding synthetic PEG-based gel will require additional biomodification to function as an effective Anisogel.

To investigate the potential of our anisotropic aECM for aligned complex tissues, we implanted chicken derived dorsal root ganglions (DRGs) into the fibrin-based gels as a model for nerve tissue (Fig. 7A). We decided to continue using GRGDS, as this ligand has a positive effect on neurite extension of chicken derived neurons (Fig. S16). These results are in agreement with reports in the literature, describing the positive character of fibronectin [58] and RGD [59] on chicken DRG growth. In addition, RGD can promote the growth of nerve supporting cells present inside the DRGs, such as Schwann cells, fibroblasts, etc. [60]. We continue with a concentration of 1 mM GRGDS in accordance to literature [55,61] and, furthermore, verify that the chosen GRGDS concentration is in a suitable range based on a 2D culture of primary neurons on a surface with the same polymer composition as the microgels (Fig. S17). Similarly to fibroblasts, nerve cells interact with the microgels in a 2D manner and do not penetrate the microgels, which have a diameter that is approximately 5 times larger than the axons. In between the microgels, the nerve extensions interact with the surrounding fibrin gel in 3D.

Interestingly, in the case of neurite growth inside the fibrin Anisogels, no significant differences between GRGDS-coupled and bioinert microgels are observed in their capability to align neurons at a minimal microgel concentration of 1 vol% (Fig. 7B). Analysis of the FWHM of the distributions portraying the direction of neuronal growth (β-tubulin, Fig. S18) shows alignment of the DRGs in both cases: bioinert microgels ($76.3 \pm 8.1^\circ$) and GRGDS-functionalized microgels ($85.0 \pm 3.9^\circ$, Fig. 7C), while randomly oriented microgels resulted in non-directed neurite extension (~171°, Fig. S19). Interestingly, the produced fibronectin follows the neuronal alignment (Fig. 7D), indicating a cell-induced synthesis of native-like oriented ECM. The density of neurite outgrowth is quantified in function of the distance from the core of the DRG (Fig. S20). Here, three different parameters are analyzed: the maximal neurite density, the distance at which this maximum drops 50%, and the distance at which no more neurite outgrowth is observed. For all these measures, no significant differences are observed between GRGDS-functionalized and bioinert microgels (Fig. 7E). This indicates neither a suppressive effect, nor an enhancing synergistic effect of GRGDS functionalized microgels on chicken neuronal growth, suggesting that the mechanical effect of the aligned microgels trumps their biochemical signaling to trigger oriented neurite growth. This observation is consistent with a recent 2D study where other cell types, such as fibroblasts or endothelial cells, were more sensitive to the physical guidance effect of aligned electrospun fiber mats compared to orthogonally patterned RGD, indicating a dominance of physico-mechanical signals over biochemical cues [62]. Aligned fibers have demonstrated to orient regenerating nerves in many applications with the fiber density (below 2.5 μm) affecting the total number of growing neurites but not the length on the extending neurites [63]. Another study found that nerve cells grow in bundles perpendicular to the fiber orientation when fibers are sufficiently close (<2.5 μm) and flexible to be pulled together [64]. Interestingly, this effect was abolished when the fibers were coated with a biological ECM protein, hinting at the importance of cell adhesion of the fibers to align cells.

In this report, the diameter of the microgels is 5 μm and the microgels are embedded inside another cell adhesive matrix. In the

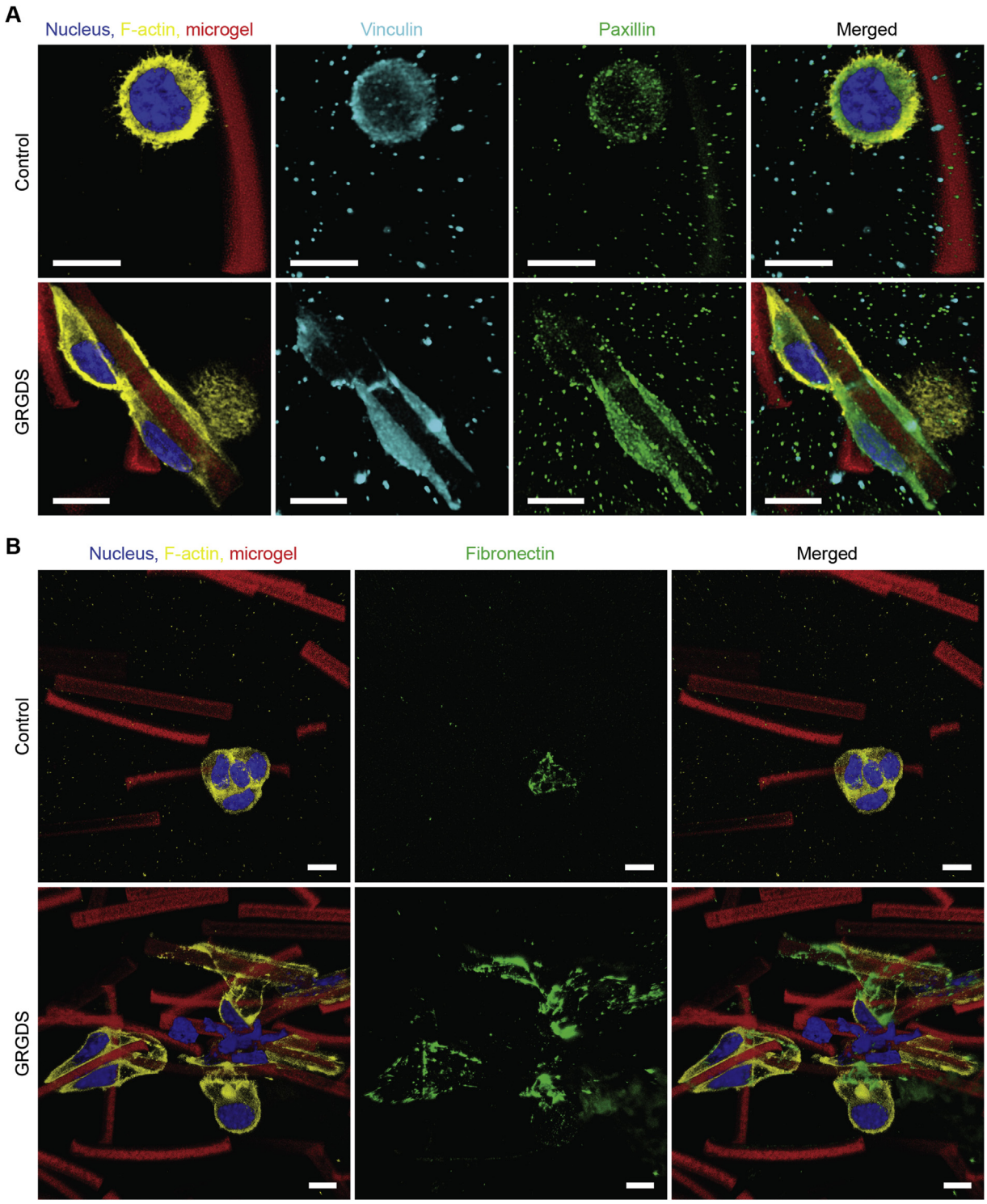

Fig. 6. Effect of biofunctionalized microgels in a synthetic bioinert PEG-based hydrogel. A) Cells spread more when in contact with bioactive microgels, whereas the cells in the control have spherical morphologies. B) Effect of microgel functionality on fibronectin production, showing a higher amount of fibronectin for biofunctionalized microgels due to a higher cell number of vital cells. Blue: nucleus, yellow: F-actin, red: microgels, turquoise: vinculin, green: paxillin. Scale bars are 10 μm. (For interpretation of the references to color in this figure legend, the reader is referred to the Web version of this article.)

case of GRGDS-microgels, small increases in neurite density and length are observed, which may be due to an enhanced biocompatibility of the material, leading to stronger interaction with the nerve supporting cells present inside the DRGs. The fact that RGD modified microgels do not significantly affect nerve alignment demonstrates that the small amounts of guiding microgels already have a dominating effect on aligning neurite growth. These results confirm that Anisogels are capable of aligning sensitive tissue cultures, such as nerve cells. Although the conjugation of GRGDS to the structural microgels only shows minor enhancements in performance, more intricate bio-ligand patterns, which mimic the natively occurring binding signals of neuronal tissues (e.g. IKVAV,

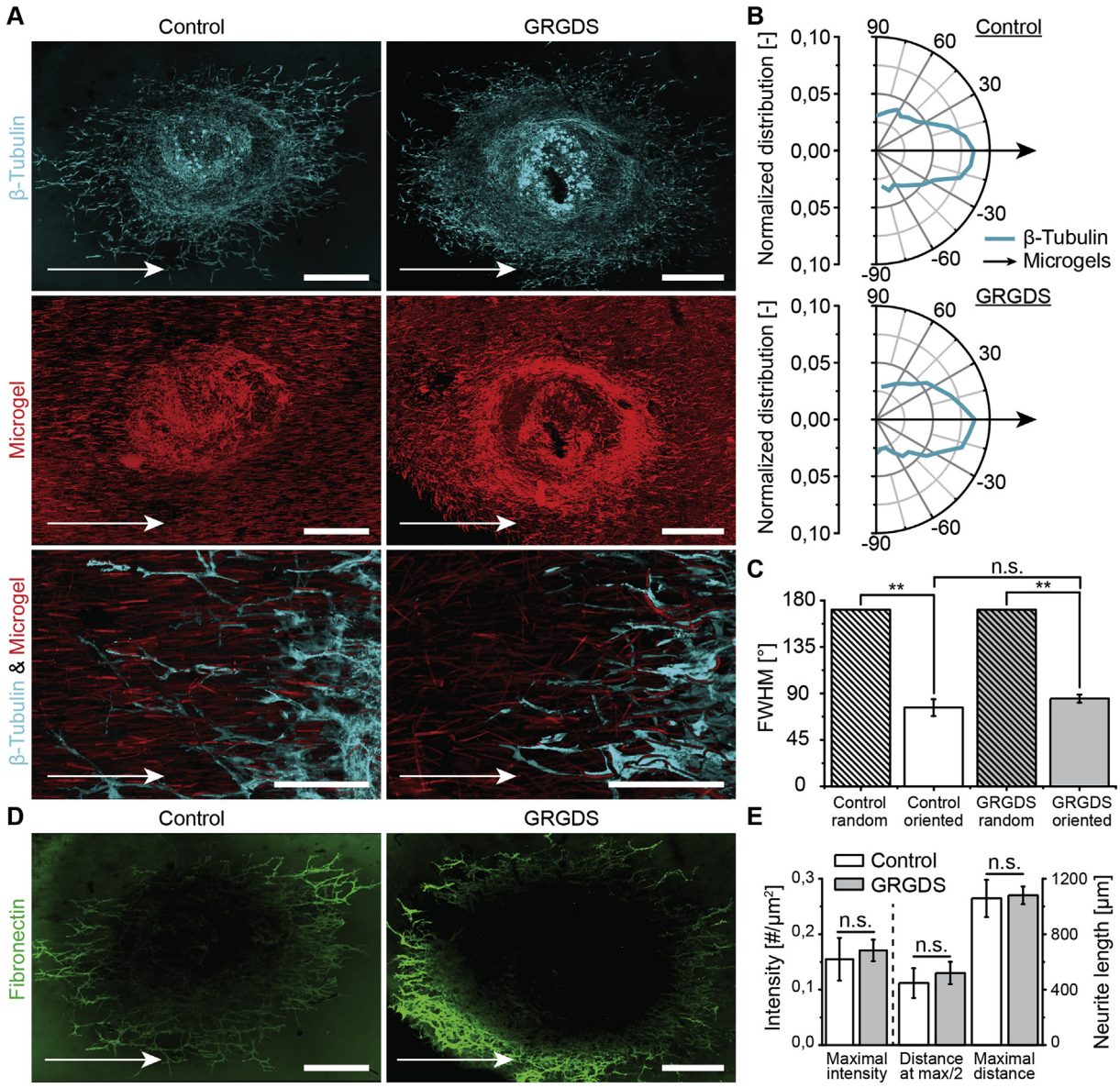

Fig. 7. The anisotropic hydrogels align neuronal DRG outgrowth and the produced ECM, independently of the biofunctionalization of the microgels. A) Neurons (turquoise) and microgels (red) with and without biofunctionalization show an aligned character, as well as the synthesized fibronectin (green) (D). B) Distribution of neurite orientation with respect to the direction of the microgels (black arrow). C) FWHM of the orientation distributions of ≥3 DRGs. E) Maximal neurite density, the distance at which this maximum drops 50%, and the distance at which no more neurite outgrowth is observed (maximal distance) inside the Anisogel containing microgels with and without conjugated GRGDS (≥3 DRGs). Data presented as average ± s.d. and statistical significance performed using one-way ANOVA with Bonferroni comparison (**$p < 0.01$; n.s. = $p > 0.05$). Turquoise: β-tubulin, red: microgels, green: fibronectin. Scale bars are 500 μm for overviews (A, B) and 200 μm for magnified images (A). White arrow indicates the direction of the previously applied magnetic field (microgel alignment). (For interpretation of the references to color in this figure legend, the reader is referred to the Web version of this article.)

YIGSR, RNIAEIIK [61]), may be beneficial as an artificial neuronal ECM.

For other hierarchical complex tissues, like cardiac tissue, a proper alignment of cells is required to provide mechanical and electrical coupling, which is facilitated by the interaction with the native ECM scaffolds. This cell-ECM communication is affected by spatial and temporal signal on different scales, ranging from nano to millimeter and nanoseconds to seconds, respectively [65,66]. Our biomaterial model aims to provide signaling cues to direct cells in a more simple and modular manner compared to native complex tissues. The individual controllability of the surrounding mechanical/biochemical properties, as well as the structural/anisotropic features in a 3D environment, allows studying these cell-material interactions in a precise way.

3. Conclusions

We established a method to biofunctionalize rod-shaped, magneto-responsive, microgels with synthetic bioactive peptides to fabricate injectable unidirectional aECMs. By presenting bioactive epitopes in a controlled manner, a novel degree of biomimicry of Anisogels is achieved, closely resembling structural proteins of the native ECM of anisotropic, hierarchical tissues.

Here, we show that cells strongly interact with biofunctionalized microgels in both a 3D natural and synthetic hydrogel. In the case of cell-adhesive fibrin, the cells prefer to interact with the bioactive microgels leading to a higher deformation of the nuclei compared to the non-modified microgels, which indicates a higher force exerted on the cell body. In addition, the

overall cell orientation is enhanced by the biochemical modification of the structural microgels, which seems to be related to an enhanced nuclear YAP-localization that increases with higher microgel contents and the addition of GRGDS. These results suggest that cells are not only affected by neighboring microgels but also by the overall anisotropy of the Anisogel.

Another striking difference, observed in the case of biofunctionalized microgels, is the reduced ECM production. Focal adhesion staining against vinculin reveals that cells indirectly interact with bioinert microgels via the production of their own ECM proteins, whereas cells covering the biofunctionalized microgels do not have to produce as much fibronectin to strongly interact with the microgels. In addition, we demonstrate that the overall production of fibronectin depends on the biochemistry of the surrounding microenvironment of the microgels. In the case of natural fibrin, less fibronectin is produced for GRGDS-coupled microgels, while in the case of synthetic PEG, biofunctional microgels are able to interact with the cells, resulting in adhesion and proliferation accompanied with an enhanced level of fibronectin production. Interestingly, the fibronectin, produced by the cells, is structurally oriented in the direction of the aligned microgels. This may result in a positive feedback cycle supporting cell guidance in a specific direction and raises the question of how much guidance we have to provide for the cells before they take over and follow the material instructions towards aligned functional tissue.

Although a positive effect of RGD on neuronal growth of DRGs is expected [59], the GRGDS-modified microgels inside a fibrin gel do not significantly affect the level of outgrowth or orientation of neurons, derived from chicken DRGs. Only a slight enhancement of neurite extension is observed for GRGDS-functionalized microgels, which may have been induced indirectly by the interaction with supporting cells. The results suggest that the signal for neuronal cell alignment coming from the anisotropic character (aligned microgels) of the Anisogel superimposes biochemical cues coming from GRGDS functionalization. Based on the presented results, the developed hybrid hydrogel can be loaded with cells and crosslink enzymatically *in situ* under physiological conditions. The Anisogel system can be applied either for *in vitro* tissue engineering applications, *ex vivo* tissue models, or *in vivo* regenerative medicine applications in a low invasive manner. The high versatility of this plug and play system provides the possibility to alter the biochemical, mechanical, and structural design properties bottom-up in a controlled manner, allowing adaptability to the complexity of different types of tissues.

4. Materials and methods

4.1. Anisometric microgel fabrication

Anisometric microgels consist of 3 kDa six-arm poly(ethylene oxide-*stat*-propylene oxide) with a ratio of 4:1 ethylene oxide to propylene oxide (sPEG) (CHT R. Beitlich GmbH). The presence of 20% propylene reduces the crystallinity of sPEG at high molecular weights, rendering the polymer liquid. Acrylate end groups are introduced by functionalization of sPEG with hydroxyl end groups using acrylic acid anhydride (Sigma-Aldrich) according to a classical Fischer esterification [67]. 101.80 g sPEG-OH (0.204 mol hydroxyl groups, 1 eq.) is dried at 80 °C for 20 h and then dissolved in 750 mL of dried toluene (Sigma-Aldrich). 24.2 g of pyridine (0.306 mol, 1.5 eq., Sigma-Aldrich) is added, followed by dropwise addition of 33.38 g acrylic acid anhydride (0.265 mol, 1.3 eq., Polysciences) at room temperature (RT). The solution is stirred for 24 h at RT and the solvent is removed under reduced pressure. The residue is taken up in dichloromethane (Sigma-Aldrich) and the product is purified by repeated precipitation steps in cold diethyl ether (Sigma-Aldrich). The degree of functionalization is determined by ^{1}H NMR analysis (>98%).

The functionalized sPEG-A, which has a density of ~1.13 g/mL, is diluted with dimethyl sulfoxide (DMSO, VWR) and a photoinitiator solution (2-hydroxy-4'-(2-hydroxyethoxy)-2-methylpropiophenone (Irgacure D-2959®, Sigma-Aldrich) in DMSO with a concentration of 0.1 mg/mL) in order to produce a 100 w/vol% sPEG-A solution with a final photoinitiator concentration of 1 mol% per free acrylate groups. In the case of fluorescent labeling, 0.05 w% of methacryloxyethyl thiocarbamoyl rhodamine B (Polysciences) is added. The final solution is mixed under exclusion of light for 4 h.

To prepare molds for the microgels, polydimethylsiloxane (PDMS, Sylgard® 184, Dow Corning) is mixed with a thermoinitiator at a ratio of 10:1 and the solution is stirred vigorously. The solution is sequentially poured on a fluorsilanized silicon wafer, containing rectangular features of $5 \times 5 \times 50$ μm. The wafer with the liquid PDMS on top is stored at RT for 1 h to ensure complete air removal before curing at 110 °C for 4 h. The cured PDMS is peeled off the wafer, forming the mold.

The microgels are fabricated as previously described [39]. For dilution of sPEG-A to a 20 w/vol% solution, 200 Da PEG-OH (Sigma-Aldrich) is added instead of water to generate a non-volatile polymer blend, which avoids evaporation during the fabrication process of the microgels. SPIONs (EMG 700, Ferrotec Europe GmbH) are dispersed in the polymer blend, which is applied to the PDMS mold with the desired cavities. A delamination step results in filled cavities with well-defined gaps (free of polymer) on the surface of the mold between the cavities. The sPEG-A is UV-crosslinked for 60 min, while the inert 200 Da PEG-OH diluent does not participate in the reaction. This causes a reaction induced phase separation, facilitating full extraction of the PEG-OH after curing. The cured microgels inside the cavities of the mold are then washed with acetone for 2 h and twice with deionized water for 30 min. The mold with the microgels is fixed upside-down on a glass slide with 50 w% polyvinylpyrrolidone (PVP, Sigma-Aldrich) in water and dried at 40 °C. After three days, the mold is peeled off the glass slide, releasing the microgels from the PVP glue, which is dissolved by deionized water to collect the microgel dispersion. The microgels are concentrated by centrifuging the solution at 4500 g for 10 min. For cell experiments, the microgels are subsequently sterilized using UV-radiation for 30 min and twice with ethanol (70 vol %), followed by washing twice with phosphate buffered saline (PBS, VWR) pH 7.4 and twice with cell media.

4.2. Biomolecule-polymer-conjugate preparation

Thiol-containing biomolecules (Cysteine (Sigma-Aldrich), Gly-Arg-Gly-Asp-Ser-Pro-Cys (GRGDSPC), Bachem) and sPEG-A are diluted in 0.1 M phosphate buffer pH 7.4 and changes in pH are adjusted to 7.4 using 1 M NaOH (Sigma-Aldrich). The solution is mixed and stirred for 10 min to enable Michael-type addition. The reaction is quenched by lowering the pH to 6.0 by adding 1 M HCl (Sigma-Aldrich). The consumption of the thiols throughout the Michael-type addition is quantified by measuring the free thiols using an Ellman's test. 12.5 μL of Ellman's solution (4 mg 5,5′-dithiobis-(2-nitrobenzoic acid) (DTNB) (Sigma-Aldrich)) in 1 mL 0.1 M phosphate buffer pH 8.0) is diluted in 625 μL 0.1 M phosphate buffer pH 8.0 to obtain the Ellman's reaction solution. The DTNB reacts with the remaining thiols, forming absorbing 2-nitro-5-thiobenzoate ($\lambda = 412$ nm). A calibration using cysteine in solution is used to determine the thiol concentrations based on the absorption.

The solvent (buffer) of the biomolecule-sPEG-conjugate is

removed via lyophilization and the product is used in weight ratios with sPEG-A for the preparation of microgels as described before. For ^{1}H NMR analysis, 15 mg of biomolecule-polymer-conjugate is dissolved in 700 μL of D_2O (Sigma-Aldrich, Bruker DPX-400 FT NMR 400 MHz spectrometer). For qualitative evaluation of the conjugation reaction, 3.0 mg activated 5-((2-(and-3)-S-(acetylmercapto) succinoyl) amino) fluorescein, containing a free thiol group (SAMSA-fluorescein, Thermo Fisher Scientific) (5.7 μmol, 0.2 eq.), or 1.9 mg fluorescein (5.7 μmol, 0.2 eq., Sigma-Aldrich) without a thiol group (negative control), are added to 15 mg sPEG-A (27.1 μmol acrylates, 1 eq.) at 1:4.7 M ratio and diluted with 85 mg sPEG-A resulting in a final SAMSA/fluorescein concentration of 11.2 mM in the microgel. Fluorescent labeling of the microgels is analyzed using microscopy (Zeiss AxioObserver Z1). To visualize the incorporation of sPEG-GRGDS conjugates into the microgels, an antibody-based staining is performed. GRGDS functionalized microgels and non-modified microgels are incubated with a primary antibody (Anti-RGD (Biorbyt), 1:100 in PBS) overnight at RT, washed three times with PBS pH 7.4, and incubated with a secondary antibody (goat anti-rabbit Alexa Fluor® 488 (Thermo Fisher Scientific), 1:100 in PBS) overnight at RT, followed by three washing steps with PBS pH 7.4.

The porous structures of microgels with and without GRGDS are compared using cryo field emission scanning electron microscopy (cryo FE-SEM, SU4800 Hitachi Ltd. Corporation). For this purpose, the swollen microgels are frozen in liquid ethane for 1 min and transferred into liquid nitrogen. The samples are cut inside the FE-SEM pre-chamber, sublimated for 10 min, and visualized at 1 kV and 1 μA. The magneto-responsiveness of the microgels with and without GRGDS is analyzed by performing an orientation assay. The orientation time of the microgels is determined as previously described [39], utilizing the tensor flow method implemented in the OrientationJ plugin of ImageJ. Briefly, the dominant orientation and coherency are determined for each video frame and microgels are considered as aligned, when the coherency, which is an indicator of the quality of the determined orientation, changes relatively less than 1%/s over a course of 5 s.

4.3. Cell culture

Mouse-derived L929-fibroblasts are cultured in RPMI media 1640 (Lonza) supplemented with 10 vol% of fetal bovine serum (FBS, Biowest) and 1 vol% Gibco™ antibiotic-antimycotic at 37 °C and 5 vol% CO_2. Dorsal root ganglia (DRGs) derived from chicken embryos (day 10) are cultivated in Dulbecco's Modified Eagle Medium (DMEM) media (Lonza), supplemented with 20 ng/mL nerve growth factor (NGF, PeproTech). To optimize the amount of bioactive GRGDS peptide in the polymer, a proliferation assay using (3-(4,5-dimethylthiazol-2-yl)-5-(3-carboxymethoxyphenyl)-2-(4-sulfophenyl)-2H-tetrazolium) (MTS, Promega) is performed. Therefore, a thin sPEG-gel film with different concentrations of GRGDS is prepared on a plasma treated 15 mm coverslip and UV cured for 1 h (Fig. S6). The sPEG-A is pre-functionalized with GRGDS as described before using 1 mg peptide (1.45 μmol, 0.18 eq.) and 4.5 mg sPEG-A (8.12 μmol acrylates, 1 eq.) and different GRGDS concentrations are achieved by mixing different weight ratios of the functionalized sPEG-GRGDS and non-functionalized sPEG-A with PEG-OH (200 Da). The total polymer concentration is kept constant at 20 w/vol%. The functionalized sPEG-gel films are washed once with acetone for 2 h and twice with MilliQ water for 30 min. After sterilization with UV-radiation for 30 min, the films are washed twice using 70 vol% ethanol. Before seeding 25,000 cells per sample, the sPEG-gel films are washed twice with PBS and RPMI media. A tissue culture polystyrene (TCPS) dish with the same surface area is used as a control. The cells are then cultivated for 72 h, after which the sPEG-films are detached from the cover slips and transferred to a new well to add MTS solution and incubate it for 4 h at 37 °C. 100 μL per sample is placed in a 96 well plate and absorption is measured at a wavelength (λ) of 490 nm using a microplate reader (Biotek® Synergy HT, USA). The absorption at 490 nm was normalized by dividing the measured absorption with the absorption of the positive control in order to analyze the metabolic activity of the cell. Additionally, a Live/Dead staining for the optimized GRGDS concentration and for a non-functionalized sPEG-based hydrogel is performed (Live/Dead® Viability/Cytotoxicity kit for mammalian cells, Biovision) [68]. Specifically, 2 μL of 2 mM Ethidium homodimer-1 in DMSO/H_2O 1:4 (v/v) and 0.5 μL of 4 mM Calcein AM in anhydrous DMSO are dissolved in 1000 μL PBS pH 7.4 and added to the cells. Samples are incubated at 37 °C for 30 min and washed with PBS. Subsequently, cells are analyzed using fluorescence microscopy ($\lambda = 530$ nm for live cells and $\lambda = 645$ nm for dead cells). For analyzing nerve growth on the sPEG-films, plasma treated cover slips ($Ø = 9$ mm) are acryl-silanized using 200 μL of 3-(Trimethoxysilyl)propyl acrylate (92% pure, Sigma-Aldrich) in an desiccator under reduced pressure for 2 h and excess of the material is removed in an empty desiccator under reduced pressure for 2 h. Subsequently, 5 μL of sPEG-films with a final concentration of 1 mM GRGDS are prepared on the functionalized cover slides and washed as described above before seeding 30,000 neurons. Neurons are cultivated for 3 days using cDMEM with 10% FBS and 13 ng/mL NGF.

In addition, to ensure that the sPEG-A does not release any cytotoxic compounds, a cytotoxic test is performed. 25 μL of sPEG-gel films are prepared and washed as described before and incubated with 1 mL media for three days (2.5 vol% sPEG-gel in media) (conditioned media). The media is removed from the gel and sequentially added to fibroblasts cultured on a TCPS surface.

To ensure that the GRGDS peptide is not deactivated by UV radiation during polymer-crosslinking, the functionality of untreated GRGDS and UV-treated GRGDS are analyzed and compared. Therefore, a previously reported method is applied [43]. In brief, amino-functionalized surfaces are PEG-coated by incubating 100 μL of 10 mg/mL sPEG-isocyanate (6 arms, $M_w = 12$ kDa) in water for 15 min at RT. Subsequently, the PEG-solution is removed and the PEG-coated surfaces are UV-sterilized for 30 min and 100 μL of the peptide solution with a concentration of 100 μM is pre-incubated for 1 h at RT. PEG-coated surfaces, coated with fibronectin (150 nM, Sigma-Aldrich), are used as a positive control, while PEG-coated surfaces without any peptides/proteins functioned as a negative control. Surfaces are UV treated for 1 h or untreated, post-cured at 4 °C overnight, and washed three times with PBS pH 7.4 to remove unbound proteins or peptides. 5000 fibroblasts per well are seeded on the surface and incubated for 3 days. Subsequently, a MTS assay is performed as described before.

For comparing full length fibronectin and GRGDS with laminin according to their ability to support neurite growth, the surfaces were coated with 150 nM laminin (29,7 μg/mL, Sigma-Aldrich) and 150 nM fibronection (33 μg/mL), as well as 100 μM GRGDS (69 μg/mL) as described above. Subsequently, DRGs from chicken embryo (day 10) are dissociated by incubation in media with 1× trypsin for 30 min at 37 °C and triturating them 20 times with a fire polished Pasteur pipette, which is repeated three times with a more narrow fire polished Pasteur pipette each time. To purify the nerve cells from fibroblasts and other non-neuronal cells, the cell solution is then placed in a large tissue culture plastic dish (small volume to area ratio) and incubated for 2 h at 37 °C to give fibroblasts and non-neuronal cells time to adhere to the surface. The nerve cells adhere much slower and, thus, most of them are still in the supernatant after 2 h incubation. After collecting them in a new vial, the supernatant is centrifuged, removed and the cell pellet

resuspended in a defined volume and counted. 15,000 nerve cells purified from dissociated nerve cells were seeded on the surface and cultivated for 3 days.

4.4. Hydrogel preparation and cultivation

For analysis of cells in the 3D hybrid Anisogels, the microgels are incorporated inside an enzymatically crosslinkable fibrin or PEG-based hydrogel. For fibrin-based hybrid hydrogels, fibroblasts in a final concentration of 500 cells per μL fibrin gel are mixed with different microgel concentrations. For the preparation of the fibrin gel, an enzyme solution is prepared (4 U/mL fibrogrammin (factor XIII, CLS Behring), 0.125 U/mL thrombin (Sigma-Aldrich), and 5 mM calcium chloride (Sigma-Aldrich) in 4-(2-hydroxyethyl)-1-piperazineethanesulfonic acid (HEPES) buffer (Life Technologies)) and incubated for 15 min at 37 °C to activate factor XIII. Subsequently, 18.2 μL of a cell-microgel-fibrinogen mixture, diluted in media (RPMI), is combined with 1.8 μL of the enzyme solution to obtain a final concentration of 8 mg/mL fibrinogen (Milan Analytica). 15 μL of the final solution is placed on a glass slide between two magnets (B = 150 mT). For DRGs, the same procedure is performed with a 15 μL hydrogel, but a final concentration of 4 mg/mL of fibrinogen is used and 20 ng/mL of nerve growth factor (NFG) supplemented DMEM is applied. The DRGs are placed on top of a cover glass inside a magnetic field and the microgel-fibrinogen mixture is pipetted on top, leading to a final SPION concentration of approximately 8 μg/mL, which is within the non-toxic range [69]. After 10 min incubation at RT, the samples are removed from the magnets and incubated for 10 min at 37 °C before adding 1 mL media. The cells are incubated at 37 °C for 3 d (fibroblasts) or 7 d (DRGs).

To decouple the matrix-cell and microgel-cell interactions, we replace the fibrin gel by a fully synthetic, bioinert PEG-hydrogel for embedding the microgels. The PEG-hydrogel is a synthetic fibrin mimic, as it uses the same enzymatic crosslinking method, using thrombin and calcium activated Factor XIII. Therefore, sPEG-conjugates are synthesized via Michael-type addition as described elsewhere [56]. Briefly, either Q- (H-NQEQVSPL-ERCG-NH2) or K-peptides (Ac-FKGG-GPQG↓IWGQ-ERCG-NH2) (Pepscan) are attached to eight-arm PEG-vinylsulfone (PEG-VS, Mw 20,000 g/mol, purchased from Jenkem technology USA Inc.) in 0.3 M triethanolamine (pH 8.0) at 37 °C for 2 h. Q- and K-peptides are added to PEG-VS in a 1.2 fold molar excess over the VS groups. Both solutions are subsequently dialyzed against double distilled water (ddH_2O) for at least 4 days at 4 °C (Slide A Lyzer, MWCO 3.5 K). After dialysis, both products ("sPEG-Q" and "sPEG-K") are obtained as a white powder after lyophilization. To confirm that the reaction is successful, ^1H NMR in D_2O is measured. The VS associated peaks at 6.3 ppm (=CH2), 6.4 ppm (=CH2), and 6.9 ppm (-SO2CH=) completely vanish in the product. Additionally, the PEG-Q arisen aromatic signals (7.1 ppm–7.6 ppm) can be attributed to the aromatic amino acids F and W, respectively, and give further evidence of the reaction. A 10 mg/mL PEG-based hydrogel (15 μL) is formed via enzymatic crosslinking between both recognition sequences in PEG-Q and PEG-K in a molar ratio of 1:1. The solution is buffered with a 10X buffer ($CaCl_2$ 0.1 M, Tris 0.5 M, NaCl 1.1 M) and crosslinks at a final concentration of 10 U/mL activated FXIII. After 10 min at RT within the applied magnetic field, the gelation is continued for 30 min at 37 °C in the incubator, followed by the addition of 1 mL media.

To analyze the difference in mechanical properties of the microgel and hydrogel components, atomic force microscopy (AFM) (Bruker, Dimension Icon FastScan System) nano-indentation is used to determine the E moduli. An s-Qube® colloidal probe (Nano and more, CP–PNPS–SiO-A-5) with a 2 μm (+/- 5%) diameter silicon dioxide sphere on a triangular gold coated cantilever is calibrated in air using the thermal resonance method built into the AFM software (spring k = 0.2467 N/m). The E-moduli are measured by indentation at 1 μm/s over an area of 5 × 5 μm and analyzed by fitting with the Hertz model (non-linear fit allowing for the simultaneous determination of the contact point and the E modulus) up to a force of 5 nN. The E modulus of the fibrin hydrogel is determined by calculating the average of all values and the E modulus of the microgels by only using the data points in the center-line of the microgel.

4.5. Immunohistochemical staining and microscopy

After cultivation, all hydrogel samples are washed for 30 min with PBS and fixed with 4% paraformaldehyde (AppliChem) for 60 min, followed by 3 washing steps (30 min) with PBS. Cells inside the gels are blocked with 4 w% bovine serum albumin (BSA, Sigma-Aldrich) in PBS for 2 h, followed by the addition of the primary antibodies against fibronectin (Sigma-Aldrich, 1:200), S100 (abcam, 1:200), paxillin (Sigma-Aldrich, 1:200), vinculin (Sigma-Aldrich, 1:100), Tuj-1 (Sigma-Aldrich, 1:250), YAP-647 (Santa Cruz Biotechnology, 1:100) or phalloidin (abcam 1:1000), which are incubated overnight at 37 °C. After washing 3 times for 30 min with PBS, secondary antibodies (Alexa Fluor 488 anti-rabbit or Alexa Fluor 633 anti-mouse (Thermo Fisher Scientific, 1:100)) are incubated for 4 h at 37 °C, after which DAPI is added for 60 min. Finally, samples are washed 3 times for 30 min with PBS and then transferred into Mowiol®, which is applied as microscopy embedding media.

2D samples are fixed with 4% paraformaldehyde for 30 min, followed by 3 washing steps (15 min) with PBS. Cells are permeabilized using 0.1% Triton-X (Sigma-Aldrich) for 3 min, washed twice with PBS and blocked with 5 w% BSA in PBS for 30 min, followed by the addition of the primary antibody against Tuj-1 (Sigma-Aldrich, 1:250) in 5 w% BSA solution, which is incubated 4 h at RT. After washing 3 times for 15 min with PBS, the secondary antibody (Alexa Fluor 488 anti-mouse, 1:100) is incubated for 1 h at RT, and, finally, samples are washed 3 times for 15 min with PBS.

Confocal laser scanning microscopy is performed with a Leica SP8 Tandem Confocal system, equipped with a white light laser (WLL). Samples are excited with the dye specific wavelengths using the WLL or a photodiode 405 in the case of DAPI. Emission is detected with PMT detectors (DAPI, microgels) or HyD detectors (fibronectin, vinculin, paxillin, phalloidin, YAP).

Images are sequentially deconvolved with Huygens Professional (Scientific Volume Imaging B.V.), performing the 'Standard' quick deconvolutions. The length and width measurements of the nuclei and cells are executed within the LasX software. Fibronectin signal quantification is performed with ImageJ by applying the 'Plot z-axis profile' and summing up the mean intensities, which are then divided by the number of cells per stack, derived from the DAPI signals. UV/VIS spectroscopic quantification of fibronectin is performed by exciting at 485/20 nm and detecting signal at 528/20 nm. Hydrogel samples are placed in the middle of a 48 well plate and area scans are executed 1 mm above the plate ground. Five measurement points (cross-shape) of the middle area are retrieved and subtracted by the mean blank values, which are hydrogels without cells. YAP-signal ratios are determined by measuring the fluorescence in a 1.5 × 1.5 μm^2 window at a random position in the nucleus and the cytoplasm and dividing the average fluorescence of each area ($F_{Nucleus}/F_{Cytoplasm}$).

The alignment of cells, DRGs, and fibronectin is quantified by first applying either a rolling ball filter with an 8-pixel ball radius (in the case of large DRG images) or no background correction. The images are sequentially smoothened with a Gaussian kernel [70]. A

locator kernel (second derivative Gaussian) is applied in one direction and a Gaussian is then rotated from 0° to 180° in 9° intervals. A threshold is applied to the maximum projection of the convoluted images along the angle axis using Otsu's method. The orientation angles (alphas) are recorded corresponding to the pixels in the maximum intensity images over the threshold and are used to generate the alpha image and the angle histogram. This diagram is rotated such that the maximum points towards 0° (Figs. S11, S13, S18).

To quantify the interaction between fibroblasts and microgels, the F-actin signal (fibroblast) and the rhodamin B signal (microgel) are analyzed in a two pass process. In the first pass, the images are summed up to create a Z-projection keeping the channels independent from each other. Here, the areas of interest are identified using a dynamic threshold, calculated by Otsu's method. Subsequently, in the second pass, the images are masked to only reveal their area of interest (defined in the first pass), then a relative intensity threshold of 0.0625 is applied to identify the pixels belonging to the valid features. This way, overlapping signals of the F-actin and the microgels are determined for all images in the z-stack (approximately 70 images) and are normalized to the F-actin signal of the cells. A series of 15 images in the z-direction, containing the highest interactions, are taken into account to determine the overall interaction between the cells and microgels. The number of analyzed samples is $n > 20$ (video 2, 3 and Fig. S7).

To quantify the neurite outgrowth from DRGs, the cores of the DRGs are cut out and the images are rendered binary by defining a threshold using Otsu's method. The images are analyzed with a MatLab code, which determines the amount of non-zero valid image pixels at a specific distance (radius) to the edge of the core. A histogram is calculated and the density of pixels is determined by dividing the number of the pixels by the area, in which they were counted. No more neurite growth is defined below a pixel density of 0.001 #/μm^2 (Fig. S20).

In order to verify the injectability of the Anisogel, a fibrin hydrogel precursor solution containing 1 vol% magneto-responsive microgels is prepared as described before. The enzyme solution is added to the mixture and a 15 μL drop is pipette on a cover slip within a 150 mT magnetic field. Laser scanning confocal imaging is performed for 2 min, followed by rotation of the magnet by 90° and further confocal imaging for 5 min.

4.6. Statistics

Analysis of statistics is conducted with OriginPro 2016G. A one-way or two-way ANOVA is performed with a post-hoc Bonferroni comparison to evaluate statistical significance ($^{*}p < 0.05$, $^{**}p < 0.01$, $^{***}p < 0.001$, $^{****}p < 0.0001$). Data are shown as mean average with error bars indicating the standard deviation.

Acknowledgements

We thank Prof. Matthias Lutolf and Delphine Blondel for their guidance in producing the PEG hydrogels. The authors thank Prof. Martin Möller for interesting scientific discussions. We are grateful to Dr. K. Rahimi, S. Moli, N. Jansen, and S. Mallmann for experimental assistance. We acknowledge funding from the European Research Council (ERC) under the European Union's Horizon 2020 research and innovation program (ANISOGEL, grant agreement No 637853), and the Deutsche Forschungsgemeinschaft (DFG) within the SFB 985 “Functional Microgels and Microgel Systems”. This work was performed in part at the Center for Chemical Polymer Technology CPT, which was supported by the EU and the federal state of North Rhine-Westphalia (grant EFRE 30 00 883 02).

Appendix A. Supplementary data

Supplementary data related to this article can be found at https://doi.org/10.1016/j.biomaterials.2018.02.001.

References

[1] Y. Luo, M.S. Shoichet, A photolabile hydrogel for guided three-dimensional cell growth and migration, Nat. Mater. 3 (4) (2004) 249–253.
[2] T.M. Keenan, A. Folch, Biomolecular gradients in cell culture systems, Lab a Chip 8 (1) (2008) 34–57.
[3] E.S. Place, N.D. Evans, M.M. Stevens, Complexity in biomaterials for tissue engineering, Nat. Mater. 8 (6) (2009) 457–470.
[4] L. De Laporte, A.L. Yan, L.D. Shea, Local gene delivery from ECM-coated poly(lactide-co-glycolide) multiple channel bridges after spinal cord injury, Biomaterials 30 (12) (2009) 2361–2368.
[5] L. De Laporte, A. Huang, M.M. Ducommun, M.L. Zelivyanska, M.O. Aviles, A.F. Adler, L.D. Shea, Patterned transgene expression in multiple channel bridges after spinal cord injury, Acta Biomater. 6 (8) (2010) 2889–2897.
[6] A.M. Kloxin, A.M. Kasko, C.N. Salinas, K.S. Anseth, Photodegradable hydrogels for dynamic tuning of physical and chemical properties, Science 324 (5923) (2009) 59–63.
[7] S.D. McCullen, H. Autefage, A. Callanan, E. Gentleman, M.M. Stevens, Anisotropic fibrous scaffolds for articular cartilage regeneration, Tissue Eng. 18 (19–20) (2012) 2073–2083.
[8] B.M. Baker, B. Trappmann, W.Y. Wang, M.S. Sakar, I.L. Kim, V.B. Shenoy, J.A. Burdick, C.S. Chen, Cell-mediated fibre recruitment drives extracellular matrix mechanosensing in engineered fibrillar microenvironments, Nat. Mater. 14 (12) (2015) 1262–1268.
[9] T. Das, K. Safferling, S. Rausch, N. Grabe, H. Boehm, J.P. Spatz, A molecular mechanotransduction pathway regulates collective migration of epithelial cells, Nat. Cell Biol. 17 (3) (2015) 276–287.
[10] J.G. Torres-Rendon, M. Köpf, D. Gehlen, A. Blaeser, H. Fischer, L.D. Laporte, A. Walther, Cellulose nanofibril hydrogel tubes as sacrificial templates for freestanding tubular cell constructs, Biomacromolecules 17 (3) (2016) 905–913.
[11] D. Zhu, H. Wang, P. Trinh, S.C. Heilshorn, F. Yang, Elastin-like protein-hyaluronic acid (ELP-HA) hydrogels with decoupled mechanical and biochemical cues for cartilage regeneration, Biomaterials 127 (2017) 132–140.
[12] T.S. Wilems, J. Pardieck, N. Iyer, S.E. Sakiyama-Elbert, Combination therapy of stem cell derived neural progenitors and drug delivery of anti-inhibitory molecules for spinal cord injury, Acta Biomater. 28 (2015) 23–32.
[13] S. Sakiyama-Elbert, J. Hubbell, Functional biomaterials: design of novel biomaterials, Annu. Rev. Mater. Res. 31 (1) (2001) 183–201.
[14] Y. Navaro, N. Bleich-Kimelman, L. Hazanov, I. Mironi-Harpaz, Y. Shachaf, S. Garty, Y. Smith, G. Pelled, D. Gazit, D. Seliktar, Matrix stiffness determines the fate of nucleus pulposus–derived stem cells, Biomaterials 49 (2015) 68–76.
[15] F. Anjum, P.S. Lienemann, S. Metzger, J. Biernaskie, M.S. Kallos, M. Ehrbar, Enzyme responsive GAG-based natural-synthetic hybrid hydrogel for tunable growth factor delivery and stem cell differentiation, Biomaterials 87 (2016) 104–117.
[16] M. Caiazzo, Y. Okawa, A. Ranga, A. Piersigilli, Y. Tabata, M.P. Lutolf, Defined three-dimensional microenvironments boost induction of pluripotency, Nat. Mater. 15 (3) (2016) 344.
[17] S. Khetan, M. Guvendiren, W.R. Legant, D.M. Cohen, C.S. Chen, J.A. Burdick, Degradation-mediated cellular traction directs stem cell fate in covalently crosslinked three-dimensional hydrogels, Nat. Mater. 12 (5) (2013) 458.
[18] D.D. McKinnon, D.W. Domaille, J.N. Cha, K.S. Anseth, Biophysically defined and cytocompatible covalently adaptable networks as viscoelastic 3D cell culture systems, Adv. Mater. 26 (6) (2014) 865–872.
[19] C. Foo, J.S. Lee, W. Mulyasasmita, A. Parisi-Amon, S.C. Heilshorn, Two-component protein-engineered physical hydrogels for cell encapsulation, Proc. Natl. Acad. Sci. U. S. A 106 (52) (2009) 22067–22072.
[20] D. Macaya, M. Spector, Injectable hydrogel materials for spinal cord regeneration: a review, Biomed. Mater. 7 (1) (2012) 012001.
[22] J.P. Vacanti, C.A. Vacanti, The history and scope of tissue engineering,, Principles of tissue engineering 3 (2000) 3–6.
[23] H. Park, J.S. Temenoff, Y. Tabata, A.I. Caplan, A.G. Mikos, Injectable biodegradable hydrogel composites for rabbit marrow mesenchymal stem cell and growth factor delivery for cartilage tissue engineering, Biomaterials 28 (21) (2007) 3217–3227.
[24] M. Whitaker, R. Quirk, S. Howdle, K. Shakesheff, Growth factor release from tissue engineering scaffolds, J. Pharm. Pharmacol. 53 (11) (2001) 1427–1437.
[25] E.J. Berns, S. Sur, L. Pan, J.E. Goldberger, S. Suresh, S. Zhang, J.A. Kessler, S.I. Stupp, Aligned neurite outgrowth and directed cell migration in self-assembled monodomain gels, Biomaterials 35 (1) (2014) 185–195.
[26] L. Cai, R.E. Dewi, S.C. Heilshorn, Injectable hydrogels with in situ double network formation enhance retention of transplanted stem cells, Adv. Funct. Mater. 25 (9) (2015) 1344–1351.
[27] S.K. Seidlits, R.M. Gower, J.A. Shepard, L.D. Shea, Hydrogels for lentiviral gene delivery, Expet Opin. Drug Deliv. 10 (4) (2013) 499–509.

[28] D.R. Griffin, W.M. Weaver, P.O. Scumpia, D. Di Carlo, T. Segura, Accelerated wound healing by injectable microporous gel scaffolds assembled from annealed building blocks, Nat. Mater. 14 (7) (2015) 737–744.
[29] A.S. Hoffman, Hydrogels for biomedical applications, Adv. Drug Deliv. Rev. 64 (2012) 18–23.
[30] X. He, E. Jabbari, Material properties and cytocompatibility of injectable MMP degradable poly (lactide ethylene oxide fumarate) hydrogel as a Carrier for marrow stromal cells, Biomacromolecules 8 (3) (2007) 780–792.
[31] M. Lutolf, J. Lauer-Fields, H. Schmoekel, A.T. Metters, F. Weber, G. Fields, J.A. Hubbell, Synthetic matrix metalloproteinase-sensitive hydrogels for the conduction of tissue regeneration: engineering cell-invasion characteristics, Proc. Natl. Acad. Sci. Unit. States Am. 100 (9) (2003) 5413–5418.
[32] T.T. Lee, J.R. García, J.I. Paez, A. Singh, E.A. Phelps, S. Weis, Z. Shafiq, A. Shekaran, A. del Campo, A.J. García, Light-triggered in vivo activation of adhesive peptides regulates cell adhesion, inflammation and vascularization of biomaterials, Nat. Mater. 14 (3) (2015) 352–360.
[33] S. Zhang, M.A. Greenfield, A. Mata, L.C. Palmer, R. Bitton, J.R. Mantei, C. Aparicio, M.O. de la Cruz, S.I. Stupp, A self-assembly pathway to aligned monodomain gels, Nat. Mater. 9 (7) (2010) 594–601.
[34] N. Dubey, P.C. Letourneau, R.T. Tranquillo, Neuronal contact guidance in magnetically aligned fibrin gels: effect of variation in gel mechano-structural properties, Biomaterials 22 (10) (2001) 1065–1075.
[35] K.J. De France, K.G. Yager, K.J.W. Chan, B. Corbett, E.D. Cranston, T. Hoare, Injectable anisotropic nanocomposite hydrogels direct in situ growth and alignment of myotubes, Nano Lett. 17 (10) (2017) 6487–6495.
[36] J. Kim, J.R. Staunton, K. Tanner, Independent control of topography for 3D patterning of the ECM microenvironment, Adv. Mater. 28 (1) (2016) 132–137.
[37] M. Antman-Passig, O. Shefi, Remote magnetic orientation of 3D collagen hydrogels for directed neuronal regeneration, Nano Lett. 16 (4) (2016) 2567–2573.
[38] E. Alsberg, E. Feinstein, M.P. Joy, M. Prentiss, D.E. Ingber, Magnetically-guided self-assembly of fibrin matrices with ordered nano-scale structure for tissue engineering, Tissue Eng. 12 (11) (2006) 3247–3256.
[39] J.C. Rose, M. Cámara-Torres, K. Rahimi, J. Köhler, M. Möller, L. De Laporte, Nerve cells decide to orient inside an injectable hydrogel with minimal structural guidance, Nano Lett. 17 (6) (2017) 3782–3791.
[40] A. Omidinia-Anarkoli, S. Boesveld, U. Tuvshindorj, J.C. Rose, T. Haraszti, L. De Laporte, An Injectable Hybrid Hydrogel with Oriented Short Fibers Induces Unidirectional Growth of Functional Nerve Cells, Small 13 (36) (2017) 8.
[41] A. Dietz, H. Rubinstein, Standardization of the ellman reaction, Clin. Biochem. 5 (1–4) (1972) 136–138.
[42] D.L. Elbert, J.A. Hubbell, Conjugate addition reactions combined with free-radical cross-linking for the design of materials for tissue engineering, Biomacromolecules 2 (2) (2001) 430–441.
[43] J. Salber, S. Grater, M. Harwardt, M. Hofmann, D. Klee, J. Dujic, H. Jinghuan, J. Ding, S. Kippenberger, A. Bernd, J. Groll, J.P. Spatz, M. Moller, Influence of different ECM mimetic peptide sequences embedded in a nonfouling environment on the specific adhesion of human-skin keratinocytes and fibroblasts on deformable substrates, Small 3 (6) (2007) 1023–1031.
[44] N. Wang, J.D. Tytell, D.E. Ingber, Mechanotransduction at a distance: mechanically coupling the extracellular matrix with the nucleus, Nat. Rev. Mol. Cell Biol. 10 (1) (2009) 75–82.
[45] D.E. Discher, P. Janmey, Y.L. Wang, Tissue cells feel and respond to the stiffness of their substrate, Science 310 (5751) (2005) 1139–1143.
[46] B. Geiger, J.P. Spatz, A.D. Bershadsky, Environmental sensing through focal adhesions, Nat. Rev. Mol. Cell Biol. 10 (1) (2009) 21–33.
[47] J. Solon, I. Levental, K. Sengupta, P.C. Georges, P.A. Janmey, Fibroblast adaptation and stiffness matching To soft elastic substrates, Biophys. J. 93 (12) (2007) 4453–4461.
[48] A. Henschen, F. Lottspeich, M. Kehl, C. Southan, Covalent structure of fibrinogen, Ann. N. Y. Acad. Sci. 408 (1983) 28–43.
[49] J. Gailit, C. Clarke, D. Newman, M.G. Tonnesen, M.W. Mosesson, R.A. Clark, Human fibroblasts bind directly to fibrinogen at RGD sites through integrin alpha(v)beta3, Exp. Cell Res. 232 (1) (1997) 118–126.
[50] K. Yokoyama, X.P. Zhang, L. Medved, Y. Takada, Specific binding of integrin alpha v beta 3 to the fibrinogen gamma and alpha E chain C-terminal domains, Biochemistry 38 (18) (1999) 5872–5877.
[51] E. Makogonenko, G. Tsurupa, K. Ingham, L. Medved, Interaction of fibrin(ogen) with fibronectin: further characterization and localization of the fibronectin-binding site, Biochemistry 41 (25) (2002) 7907–7913.
[52] A. Sahni, T. Odrljin, C.W. Francis, Binding of basic fibroblast growth factor to fibrinogen and fibrin, J. Biol. Chem. 273 (13) (1998) 7554–7559.
[53] M.M. Martino, P.S. Briquez, A. Ranga, M.P. Lutolf, J.A. Hubbell, Heparin-binding domain of fibrin (ogen) binds growth factors and promotes tissue repair when incorporated within a synthetic matrix, Proc. Natl. Acad. Sci. Unit. States Am. 110 (12) (2013) 4563–4568.
[54] G. Halder, S. Dupont, S. Piccolo, Transduction of mechanical and cytoskeletal cues by YAP and TAZ, Nat. Rev. Mol. Cell Biol. 13 (9) (2012) 591–600.
[55] L.A.S. Callahan, E.P. Childers, S.L. Bernard, S.D. Weiner, M.L. Becker, Maximizing phenotype constraint and extracellular matrix production in primary human chondrocytes using arginine-glycine-aspartate concentration gradient hydrogels, Acta Biomater. 9 (7) (2013) 7420–7428.
[56] M. Ehrbar, S.C. Rizzi, R. Hlushchuk, V. Djonov, A.H. Zisch, J.A. Hubbell, F.E. Weber, M.P. Lutolf, Enzymatic formation of modular cell-instructive fibrin analogs for tissue engineering, Biomaterials 28 (26) (2007) 3856–3866.
[57] Y. Wu, K.J. Grande-Allen, J.L. West, Adhesive peptide sequences regulate valve interstitial cell adhesion, phenotype and extracellular matrix deposition, Cell. Mol. Bioeng. 9 (4) (2016) 479–495.
[58] A.M. Hopkins, L. De Laporte, F. Tortelli, E. Spedden, C. Staii, T.J. Atherton, J.A. Hubbell, D.L. Kaplan, Silk hydrogels as soft substrates for neural tissue engineering, Adv. Funct. Mater. 23 (41) (2013) 5140–5149.
[59] N.H. Romano, C.M. Madl, S.C. Heilshorn, Matrix RGD ligand density and L1CAM-mediated Schwann cell interactions synergistically enhance neurite outgrowth, Acta Biomater. 11 (2015) 48–57.
[60] E. Frank, J.R. Sanes, Lineage of neurons and glia in chick dorsal root ganglia: analysis in vivo with a recombinant retrovirus, Development 111 (4) (1991) 895–908.
[61] J.C. Schense, J. Bloch, P. Aebischer, J.A. Hubbell, Enzymatic incorporation of bioactive peptides into fibrin matrices enhances neurite extension, Nat. Biotechnol. 18 (4) (2000) 415–419.
[62] R.J. Wade, E.J. Bassin, W.M. Gramlich, J.A. Burdick, Nanofibrous hydrogels with spatially patterned biochemical signals to control cell behavior, Adv. Mater. 27 (8) (2015) 1356.
[63] H.B. Wang, M.E. Mullins, J.M. Cregg, A. Hurtado, M. Oudega, M.T. Trombley, R.J. Gilbert, Creation of highly aligned electrospun poly-L-lactic acid fibers for nerve regeneration applications, J. Neural. Eng. 6 (1) (2009) 016001.
[64] J.W. Xie, W.Y. Liu, M.R. MacEwan, P.C. Bridgman, Y.N. Xia, Neurite outgrowth on electrospun nanofibers with uniaxial alignment: the effects of fiber density, surface coating, and supporting substrate, ACS Nano 8 (2) (2014) 1878–1885.
[65] S.F. Badylak, D.O. Freytes, T.W. Gilbert, Extracellular matrix as a biological scaffold material: structure and function, Acta Biomater. 5 (1) (2009) 1–13.
[66] K.K. Parker, D.E. Ingber, Extracellular matrix, mechanotransduction and structural hierarchies in heart tissue engineering, Philosophical transactions of the Royal Society of London, Series B, Biological sciences 362 (1484) (2007) 1267–1279.
[67] D.E. Bergbreiter, G. Tao, A.M. Kippenberger, Functionalized hyperbranched polyethylene powder supports, Org. Lett. 2 (18) (2000) 2853–2855.
[68] M. Probes, LIVE/DEAD® Viability/Cytotoxicity Kit* for Mammalian Cells*, MP, 2005.
[69] N. Singh, G.J.S. Jenkins, R. Asadi, S.H. Doak, Potential toxicity of superparamagnetic iron oxide nanoparticles (SPION), Nano Rev. 1 (2010), 10.3402/nano.v1i0.5358.
[70] D. Missirlis, T. Haraszti, C.V.C. Scheele, T. Wiegand, C. Diaz, S. Neubauer, F. Rechenmacher, H. Kessler, J.P. Spatz, Substrate engagement of integrins α5β1 and αvβ3 is necessary, but not sufficient, for high directional persistence in migration on fibronectin, Sci. Rep. 6 (2016) 23258.